Available online at www.sciencedirect.com
SCIENCE DIRECT®
Journal of Sound and Vibration 270 (2004) 233–257
JOURNAL OF SOUND AND VIBRATION
www.elsevier.com/locate/jsvi

Transient turbulent friction in fully rough pipe flows

A.E. Vardy*, J.M.B. Brown

Civil Engineering Department, School of Engineering, University of Dundee, Dundee DD1 4HN, UK

Received 5 July 2002; accepted 8 January 2003

Abstract

A weighting-function model of unsteady skin friction in fully rough-walled flows in one-dimensional ducts is derived using an idealized radial viscosity distribution. The model complements previous work by the authors for smooth-walled flows. It is assumed that, for sufficiently short-lived transients, the viscosity distribution in the cross-section may be regarded as constant and equal to that in a pre-existing steady flow. The eddy viscosity in an outer annulus is assumed to vary linearly from a minimum at the wall to a maximum at the edge of a central core of uniform viscosity. The resulting weighting-function model for short-lived transients is used to develop a simple formula predicting values of unsteady skin friction coefficients suitable for an instantaneous-acceleration model of unsteady skin friction in fully rough pipe flows.

1. Introduction

Skin friction forces on pipe walls during and after rapid rates of change of velocity can greatly exceed values predicted using quasi-steady formulae based on instantaneous flow speeds [1,2]. The effect is especially important when steep-fronted pressure waves exist. Typical examples include water-hammer waves following rapid valve closures [3] and pseudo-shock waves in tunnels due to the passage of very fast trains [4].

It is convenient to regard the total wall shear stress at any instant as the sum of two components. That is,

$$\tau_w = \tau_{ws} + \tau_{wu}, \tag{1}$$

where τ_{ws} is the quasi-steady value based on the instantaneous velocity and τ_{wu} is an additional contribution due to unsteadiness. Extensive information exists to enable the amplitude of the first

*Corresponding author. Tel./fax: +44-1828-686065.
E-mail address: a.e.vardy@dundee.ac.uk (A.E. Vardy).

0022-460X/03/$ - see front matter
doi:10.1016/S0022-460X(03)00492-9

of these components to be estimated, based on empirically determined skin friction coefficients whose values can usually be estimated with good accuracy. In contrast, very little information exists about likely values of the time-dependent component τ_{wu}.

The purpose of this paper is to provide a method of estimating values of τ_{wu} without recourse to empirical data other than that which are already needed for the estimation of the quasi-steady contribution τ_{ws}. The authors have previously provided such a method for smooth-walled turbulent flows, but this is believed to be the first time that one has been offered for rough-walled flows.

The origins of the methodology used herein can be attributed to Zielke [1], who, for the special case of laminar flow, obtained an exact relationship between the unsteady component of the wall shear stress and a weighted integral of the acceleration history of the mean flow.

In most laminar flows, the viscosity may be regarded as uniform in space and constant in time. In *steady* turbulent flows, it is non-uniform in space, but constant in time. In *unsteady* turbulent flows, it is both non-uniform and non-constant. This behaviour greatly complicates the prediction of wall shear stresses and, with today's understanding, there would be no possibility of obtaining meaningful analytical solutions without recourse to simplifying assumptions. Herein, a plausible approximation is used to represent the non-uniformity, but no account is taken of temporal variations in the viscosity. The justification for these simplifications is presented in Section 3. First, however, it is useful to summarize previous important studies of unsteady skin friction in pipes.

1.1. Previous work: smooth-walled flows

Ohmi and Usui [5] defined time-invariant approximations to eddy viscosity distributions in pipes, based on experimental data obtained for steady state flows. The approximations were expressed as empirical relationships applicable in successive radial regions. Using them, the governing flow equations were integrated numerically to obtain velocity profiles and wall shear stresses in oscillating flows in smooth-walled pipes. A four-region model that performed well was subsequently used by Ohmi et al. [6] to simulate unsteady, non-oscillating flows.

Eichinger and Lein [7] used a k–epsilon model to represent the turbulence structure in the momentum equation. This has the important advantage of enabling account to be taken of time dependence of the viscosity. They used their model together with the method of characteristics to obtain numerical solutions of various unsteady flows in pipelines, obtaining good agreement of amplitude and phase with experimental measurements.

The above methods are powerful, but they have the crucial disadvantage of requiring solutions in the plane of the cross-section simultaneously with solutions in the axial direction. This imposes very large time penalties for the analysis of transient flows in pipes. Vardy et al. [8] sought to overcome this disadvantage by developing a Zielke-like weighting-function model of transient skin friction [1]. They represented the flow in a manner suggested by Wood and Funk [9], namely as a laminar annulus adjacent to the pipe wall and a central core of uniform velocity (this implies an infinite viscosity in the core region). The governing equations were solved to derive a general function relating instantaneous wall shear stresses to historical values of the *mean* velocity of flow.

Vardy and Brown [10] subsequently presented an improved form of the above model in which the viscosity is assumed to vary linearly across the outer annular shear layer, but is constant in time. Predictions based on the resulting weighting-function have been found by other authors to compare well with experimental measurements of water hammer and with CFD analyses.

Recently [11], the model has been further refined by regarding the core as a region of uniform viscosity rather than one of infinite viscosity and uniform velocity. The revised model is shown in Section 3 to be a reasonable approximation to steady, turbulent flows that are used to define the 'frozen' viscosity state.

Zarzycki [12] has derived a weighting function using a more detailed description of the smooth pipe eddy viscosity distribution (using four, rather than two, regions). In particular, better account is taken of the viscosity distribution in the buffer zone close to the wall. The resulting analysis is too complex for use in general solutions of unsteady flows in pipes, but it provides valuable confirmation of the acceptability of the authors' coarser representation of the viscosity distribution. At short historical times, Zarzycki's more detailed approximation yields the same results as the authors' model. At large Reynolds numbers, it predicts a greater dependence on historical velocity changes, but the differences are sufficiently small to be neglected for practical purposes.

1.2. Previous work: rough-walled flows

The above methods were initially developed for smooth-walled flows. In contrast, Silva-Araya and Chaudhry [13] have presented a method that can be applied to either smooth- or rough-walled flows. They use a mixing length model of turbulence to close the equations. A numerical solution then yields a velocity distribution, from which a measure of the rate of energy dissipation can be derived. Their model has the advantage of generality, but the disadvantage of being computationally expensive. Also, although their examples show a good representation of maximum amplitudes and wave shapes, there are discrepancies in phase.

Pezzinga [14] has used a quasi-two-dimensional (2D) model to predict shear stresses in smooth- or rough-walled flows. Two regions of flow are considered, namely a turbulent core and a laminar annulus representing a viscous sublayer. A mixing length approach is used to provide the closure of the turbulence equations. The pipe is discretized cylindrically and the method of characteristics is used in the axial direction. A set of velocity distributions results, from which the wall shear stress can be calculated. When the roughness height is smaller than the viscous layer thickness, the conditions are assumed smooth. When it is greater, they are assumed rough. The method also provides for intermediate roughness conditions.

The method is more computationally expensive than one-dimensional (1D) methods, but it has been shown to give good agreement with experimental measurements. Also, it has been used to illustrate the dependence of unsteady friction on both Reynolds number and roughness [15]. For the particular case of smooth-walled flows, it has been used by Mansour et al. [16] for comparisons with experiments for Reynolds numbers up to 60 000.

1.3. Instantaneous-acceleration methods

From the point of view of analysts of unsteady flows in pipe networks, a user-friendly model of unsteady skin friction should relate the wall shear to 1D flow parameters. Several of the above methods do not do this and the remainder require extensive historical information about flow conditions. All require more computer memory than is needed for quasi-steady representations of skin friction.

Trikha [17] and Ghidaoui and Mansour [18] have presented ways of reducing this problem by approximating the historical dependence, but most analysts prefer to neglect the dependence altogether. That is, they assume that the unsteady contribution τ_{wu} depends only upon the *instantaneous acceleration* of the mean flow. The most popular model using this approach is due to Brunone et al. [19]. Some theoretical justification for the approach is provided by Axworthy et al. [20], who considered the non-equilibrium thermodynamics of the transient mechanical process and demonstrated a functional dependence of the unsteady friction on instantaneous temporal and convective accelerations of the mean flow.

Instantaneous-acceleration methods are not suitable for detailed studies of very rapid transients, but they have proved highly successful for slower transients. They are especially effective when the acceleration time scales of the physical events are long in comparison with the decay times of the unsteady component of the shear stress τ_{wu}. These time scales are quantified in Section 5 herein.

The adoption of the instantaneous-acceleration approach carries an important penalty, namely the need to introduce an empirical coefficient whose value must, in principle, be determined from experiments. An unexpected, but highly valuable benefit of weighting-function analyses has been the theoretical quantification of this coefficient. For smooth-walled flows, the present authors showed that the coefficient decreases as the Reynolds number increases [21]. Bergant et al. [22,23], Bughazem and Anderson [24] and Vitkovsky et al. [25] used these smooth-walled data in numerical predictions based on the instantaneous-acceleration method. They showed reasonable agreement with experimental measurements even though fully smooth conditions might not have existed.

Brunone et al. [26] presented data for rough-walled flows in a long pipeline ($D = 0.25$ m, $k_s = 2.2$ mm) for a range of Reynolds numbers from 240 000 to 390 000. They made comparisons with theoretical predictions using the instantaneous-acceleration method and obtained good agreement of the overall damping of pressure amplitudes. They offered the tentative conclusion that values of k_3 based on the above *smooth*-walled predictions might also be useful in *rough*-walled flows. On close inspection of rapid pressure changes, however, there is evidence that the predicted unsteady contribution to skin friction underestimates the wave dissipation. That is, the measurements imply that larger values of k_3 might apply in rough-walled flows.

1.4. Outline

The objectives of this paper are: (i) to provide a weighting-function model of fully rough-walled flows equivalent to the smooth-walled counterpart [11] and (ii) to use it to predict theoretical values of the empirical coefficient k_3 needed by users of Brunone's instantaneous-acceleration method. The development begins with an assessment of viscosity distributions in rough-walled flows and then continues in the manner used previously for smooth-walled flows. The mathematical derivation is summarized in Appendices A and B.

2. Smooth- and rough-walled conditions

Schlichting [27] gives a clear summary of a definitive investigation of *steady* flows in rough-walled pipes undertaken by Nikuradse. The pipe walls were coated with closely sized sand grains

to give a good approximation to a uniform roughness. The steady state skin friction coefficient f_s defined by

$$f_s \equiv \frac{\tau_{ws}}{\frac{1}{2}\rho U^2} \tag{2}$$

was found to depend upon the roughness size k_s and the Reynolds number **Re**, defined herein as

$$\mathbf{Re} \equiv \frac{UD}{\nu_l}, \tag{3}$$

where U is the mean velocity, D is the pipe diameter and ν_l is the laminar kinematic viscosity. In general, $f_s = f_s\{\mathbf{Re}, k_s\}$. When the influence of roughness is sufficiently small, however, the dependence reduces to $f_s = f_s\{\mathbf{Re}\}$ and, when it is large, the dependence reduces to $f_s = f_s\{k_s\}$. Expressions presented by Schlichting [27] for these extreme cases may be written as

$$\textit{Fully smooth}: \quad \frac{1}{\sqrt{4f_s}} = 2\log(\mathbf{Re}\sqrt{4f_s}) - 0.8, \tag{4}$$

$$\textit{Fully rough}: \quad \frac{1}{\sqrt{4f_s}} = 1.14 - 2\log\left(\frac{k_s}{D}\right). \tag{5}$$

These characteristic dependencies exist at sufficiently small and large values of a roughness Reynolds number k_s^+ defined by

$$k_s^+ \equiv \frac{k_s u_*}{\nu_l} = \frac{k_s}{D}\mathbf{Re}\sqrt{f_s/2}, \tag{6}$$

where u_* is the friction velocity

$$u_* \equiv \sqrt{\tau_{ws}/\rho} = U\sqrt{f_s/2}. \tag{7}$$

Experiment shows that smooth-walled behaviour $f_s = f_s\{\mathbf{Re}\}$ exists when k_s^+ is smaller than about 5 and that rough-walled behaviour $f_s = f_s\{k_s\}$ exists when k_s^+ is greater than about 70. The authors' previous papers dealt with the lower range and led to quantitative expressions for unsteady skin friction coefficients. This paper deals with the higher range and leads to a functionally different behaviour. It is hoped that a unifying methodology will be developed in due course for the intermediate range where conditions do not approximate to fully smooth or to fully rough.

Practical roughness differs from the highly regular sand grain form used by Nikuradse. Nevertheless, the same asymptotic behaviour is found and it is usual to define an "equivalent" roughness size by mapping the large-**Re** ends of the $f_s = f_s\{\mathbf{Re}, k_s\}$ curves to Nikuradse's data.

3. Idealized viscosity distribution

3.1. Smooth-walled flows

Fig. 1 shows experimental data obtained by Laufer [28] for steady, turbulent, smooth-walled pipe flows. There is an outer region of strongly varying viscosity and an inner core of approximately uniform viscosity. The variation in viscosity across the annular region is very large.

At a Reynolds number of $\mathbf{Re} = 10^5$, for example, the core viscosity is more than 150 times greater than the laminar value that exists at the wall. With the chosen axes, the data appear to collapse onto a single curve, thus implying that the kinematic viscosity scales with the friction velocity u_*

In the authors' smooth-walled analysis [11], the viscosity distribution is approximated by a bi-linear distribution depicted in Fig. 1. Using the co-ordinate systems shown in Fig. 2, there is a linearly varying viscosity within an outer annulus $0<y<b$ and a uniform viscosity within the core region $0<r<R-b$. The assumed width of the outer annulus is defined by

$$\beta = b/R, \tag{8}$$

where β is taken to be 0.2, and the kinematic eddy viscosity in the core region is defined through

$$N_c \equiv \frac{v_c}{u_* R}, \tag{9}$$

where N_c is taken as 0.065. The bi-linear approximation is coarse, but it captures the most important features of the behaviour in the annulus and core regions.

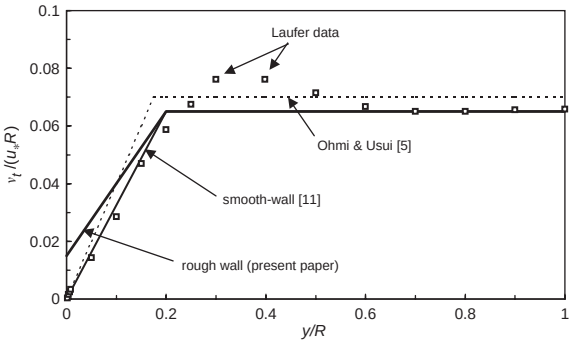

Fig. 1. Comparison of idealized turbulent kinematic viscosity distributions with measurements by Laufer for smooth-walled flows.

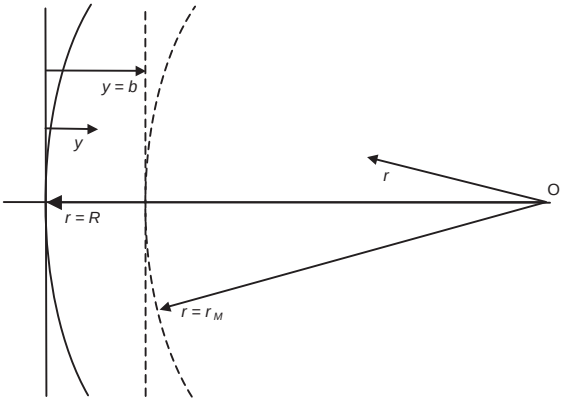

Fig. 2. Co-ordinate systems in the annulus and the core.

A disadvantage of this distribution is that it is inconsistent with the skin friction coefficient obtained from Eq. (4). The authors [10] originally overcame this problem by allowing the width of the annulus to vary. In some cases, however, the implied width was unrealistically large so the above approach (i.e., prescribing the annulus width to be $b/R = 0.2$) was subsequently adopted [11]. Consequential errors in the implied quasi-steady shear stresses were accepted because their influence on predicted values of the unsteady components of shear stress were found to be small.

3.2. Rough-walled flows

Churchill and Chan [29] noted an absence of data for rough-walled pipe flows equivalent to Laufer's data for smooth-walled flows except for extremely large roughness conditions. They pointed out, however, that, away from the immediate vicinity of the rough surface, the eddy viscosity can be determined using the same relations as for smooth pipes. Remote from the wall, the influence of roughness is exerted implicitly through the friction velocity. Herein, therefore, the width of the annulus is again assumed to be $0.2R$ and the viscosity in the core region is again assumed to satisfy Eq. (9) with $N_c = 0.065$.

In common with the smooth-walled approach, the viscosity is assumed to vary linearly across the annulus. At the wall, however, the effective viscosity is greater than the laminar viscosity, but by an unknown amount. Herein, its value is chosen to ensure that the rough-walled skin friction relationship (Eq. (5)) is satisfied, thereby avoiding the complication associated with the equivalent viscosity distribution in smooth-walled flows.

Mathematically, the viscosity distribution for any particular value of the roughness size k_s is determined in three steps. First, the viscosity in the core region is deduced from Eqs. (5), (7) and (9), using $N_c = 0.065$. Then the viscosity ratio across the annulus is determined iteratively from Eqs. (B.4)–(B.6) in Appendix B. Finally, the required viscosity at the wall is obtained as the ratio of these two values.

In the idealization used in the preceding paragraphs, the position of $r = R$ (and hence $y = 0$) is regarded as independent of k_s and the viscosity at this location is assumed to exceed the laminar viscosity. An alternative way of modelling the increased viscosity at the wall would be to imagine that the same non-dimensional viscosity distribution exists for all roughness sizes at any particular Reynolds number, but that the effective wall position moves radially inwards (i.e., 'up' the viscosity hill) as the roughness size increases. Since the precise location of $r = R$ involves non-geometrical arguments anyway, this might offer a valid way of defining the wall position mathematically. The former method is preferred herein, however, because it enables the value of β to be treated formally as independent of k_s.

3.3. Viscosity ratios

Several viscosity ratios have characteristic influences over the flow behaviour. For example, the ratio of the core viscosity to the laminar viscosity is an indicator of the increase in steady flow resistance in comparison with that which would obtain if laminar conditions could exist at the same Reynolds number. Similarly, the ratio of the core and wall viscosities has an important influence on the amplitudes of the unsteady contributions to the wall shear stress and on the rates at which these stresses decay following a sudden change in the flow conditions. The ratio of the

effective wall viscosity to the laminar viscosity is a measure of the dissipating effect of the surface roughness. Herein, viscosity ratios are expressed by the symbol σ. For example,

$$\sigma_{cw} = \frac{v_c}{v_w}, \quad \sigma_{cl} = \frac{v_c}{v_l} \quad \text{and} \quad \sigma_{wl} = \frac{v_w}{v_l}, \tag{10}$$

in which the suffices of σ define the particular ratio.

In the particular case of smooth-walled flows, $v_w = v_l$ and so the last item in Eq. (10) is simply unity. More important, the first two items are equal and, in the authors' smooth-walled paper [11], they were denoted simply by σ_c.

Using Eqs. (7), (9) and (10), the ratio of the core and laminar viscosities can be shown to satisfy

$$\sigma_{cl} \equiv v_c/v_l = N_c \, \mathbf{Re} \sqrt{f_s/8}. \tag{11}$$

Under fully rough conditions, f_s becomes independent of **Re** and so, for constant N_c, the core viscosity ratio σ_{cl} becomes proportional to **Re**. This is an important result because this ratio has a determining influence on the following analysis for unsteady skin friction. As a consequence, *unsteady* skin friction coefficients in fully rough flows are influenced by the Reynolds number as well as by the roughness size. In contrast, the *quasi-steady* coefficients depend only on the roughness size, not on the Reynolds number.

3.4. Time-dependent vicosity

The idealized viscosity distribution defined in the preceding sections has been justified only for steady state flows. Herein, however, it is also used for unsteady flows. Moreover, once chosen, the assumed viscosity distribution is regarded as 'frozen' for the duration of the analysis. Naturally, this cannot be an exact representation of physical reality, but there are strong physical, mathematical and pragmatic reasons for assuming it to be so. These reasons—and some experimental justification for them—are discussed in the authors' smooth-walled paper [11]. For sufficiently small times, the assumption is consistent with the following experimental evidence.

Early experiments reported by Maruyama et al. [30] showed evidence of delays in the change of turbulence characteristics during transient processes. Shortly after a step increase in velocity, the dominant feature was the generation and propagation of new turbulence. After a step decrease, the dominant feature was the decay of old turbulence. In both cases, the rate of change from old to new turbulence conditions was governed primarily by the conditions prevailing *before* the change.

He and Jackson [31,32] have also observed this effect. They compared experimental measurements with theoretical predictions using a CFD code with alternative models of the eddy viscosity. For short times after the commencement of the acceleration, predictions based on frozen-viscosity assumptions gave very close agreement. In contrast, predictions based on eddy viscosities linked to instantaneous flow conditions performed relatively poorly. At longer times after the commencement of the acceleration, these situations reversed. The duration of the frozen-viscosity behaviour was comparable with the duration of limit times discussed in Section 5 herein.

This behaviour is consistent with a simple interpretation. Soon after the acceleration commences, there is insufficient time for radial vorticity diffusion to influence much of the cross-section. During this period, the velocity distribution is determined primarily by the initial

viscosity distribution and the subsequent inertial disturbance. At later times, the radial diffusion will have influenced the whole of the cross-section, thereby changing the viscosity distribution. Simultaneously, inertial effects will have reduced in importance because the initial *change* of acceleration will have been 'forgotten'.

4. Unsteady flow in a rough-walled pipe

The analytical development of the weighting-function method for rough-walled flows closely follows the corresponding development for smooth-walled flows [11]. The main features are outlined below with special reference to rough-walled flows. Fuller details are presented in Appendices A and B.

First, conditions in the annulus and core regions are analyzed independently using the co-ordinate systems shown in Fig. 2. Polar co-ordinates are used in the core region where the viscosity is uniform, but plane geometry is used in the annular region where it is non-uniform. In both regions, all parameters are uniform in the axial direction. The axial pressure gradient may vary in time, but, at any instant, it is uniform in space, both axially and radially.

The governing equations are solved in the Laplace domain where time is represented by a parameter, s, not by an independent variable. This is one reason for considering early-time flows with frozen-viscosity distributions. If the viscosity varied in both time and space, Laplace transforms could not be used.

Solutions obtained independently in the annulus and core regions are matched by requiring continuity of velocity and shear stress at their common interface. The resulting velocity distributions enable an analytical expression to be determined for the Laplace transform of the total wall shear stress, namely τ'_w, which includes the steady and unsteady components. This is expressed as a function of the mean velocity over the whole cross-section.

The analysis is then repeated for a steady flow with the same instantaneous velocity and the same frozen viscosity, enabling an equivalent expression to be obtained for the quasi-steady shear stress, τ_{ws}. The unsteady contribution to the shear stress follows by subtracting the Laplace transform of τ_{ws} from τ'_w, giving

$$\tau'_{wu} = \tau'_w - \tau'_{ws}, \tag{12}$$

in which the primes denote Laplace transforms. The use of the same (frozen)-viscosity distribution for both steady and unsteady calculations is essential in order to make the use of Eq. (12) meaningful. The purpose of the analysis is to estimate the unsteady contribution. The quasi-steady analysis is not recommended for wider use in its own right.

4.1. The weighting function

In his far-sighted analysis of unsteady skin friction in laminar flows, Zielke [1] related the unsteady component of the wall shear stress to the acceleration history through a weighted integral

$$\tau_{wu} = \frac{2\rho\nu_l}{R} \int_\theta^T W\{T-\theta\} \frac{\partial U}{\partial t} \mathrm{d}\theta, \tag{13}$$

in which W is a weighting function and T is the elapsed time since the flow was stationary. The parameters t and θ are times measured forwards and backwards, respectively, so that $t+\theta=T$. The instant at which τ_{wu} is to be evaluated is denoted by $t=T$ and $\theta=0$, whereas the last instant when the flow was stationary is denoted by $t=0$ and $\theta=T$.

In the Laplace domain, the transform of the unsteady component of the wall shear stress is related to the transformed acceleration and the transformed weighting function by the relation

$$\tau'_{wu}=\frac{2\rho v_1 W'}{R}\left(\frac{\partial U}{\partial t}\right)'. \tag{14}$$

An equivalent turbulent flow relationship for unsteady flows in rough-walled pipes may be obtained by subtracting Eq. (B.8) from Eq. (A.21). Since, for zero initial velocity,

$$sU'=\left(\frac{\partial U}{\partial t}\right)'. \tag{15}$$

in which s is the Laplace transform variable, the result may be expressed as

$$\tau'_{wu}=\frac{\rho v_w \Phi_u}{s}\left(\frac{\partial U}{\partial t}\right)'. \tag{16}$$

The function Φ_u in this equation satisfies

$$\Phi_u \equiv \sqrt{\frac{s}{v_w}}[C_1 \mathrm{I}_1(\sqrt{\zeta})-C_2\mathrm{K}_1(\sqrt{\zeta})]G-\frac{1}{2v_w}[R+b]G_s, \tag{17}$$

where C_1, C_2, G, G_s and ζ are defined in Appendices A and B and I_1 and K_1 are modified Bessel's functions.

By comparing Eqs. (14) and (16), the weighting-function transform for rough-walled turbulent flows is

$$W'\{s\}=\frac{R}{2}\frac{v_w}{v_l}\frac{\Phi_u}{s} \quad \text{or} \quad W'\{s\}=\frac{R\sigma_{wl}\Phi_u}{2s}, \tag{18}$$

in which the curly brackets indicate functional dependence.

4.2. Approximate weighting function

In principle, the required weighting function is the inverse Laplace transform of Eq. (18). In practice, it would be difficult to obtain this transform and, in any case, the result would involve an infinite series of exponential terms. For the principal intended users of the weighting function, the result would be unusable, as would a numerical inverse transform.

Fortunately, a good approximation to the transformed weighting function (Eq. (18)) is given by a simpler expression for which a usable inverse transform can be evaluated, namely

$$W'_a\{s\}=\frac{A}{\sqrt{s+B}}, \tag{19}$$

in which the suffix a indicates that W'_a is approximate. Since A and B are constants for particular values of Reynolds number and roughness, the inverse transform of Eq. (19) is simply

$$W_a\{\theta\} = \frac{A\exp(-B\theta)}{\sqrt{\pi\theta}}. \tag{20}$$

The constants A and B are determined by matching the asymptotic values of Eqs. (18) and (19). A comparison as s tends to infinity leads to

$$A = \frac{R\sqrt{\nu_w}}{2\nu_l} \tag{21}$$

and a match as s tends to zero then yields the value of B, namely

$$B = (A/W'_0)^2, \tag{22}$$

in which W'_0 denotes the limiting value of Eq. (18) as s tends to zero.

This method of determining values of A and B ensures that the exact and approximate weighting functions are identical at the limits of large and small s. Between these limits, the approximation is not exact, but it is a sufficiently close fit for practical purposes.

4.2.1. *Non-dimensional form of the weighting function*

It is convenient to express A and B in non-dimensional form using

$$A^* = A\frac{\sqrt{\nu_l}}{R\sqrt{\pi}} \quad \text{and} \quad B^* = B\frac{R^2}{\nu_l}. \tag{23}$$

By also using a non-dimensional historical time ψ and a shear decay coefficient C^*, defined by

$$\psi \equiv \frac{\nu_l\theta}{R^2} \quad \text{and} \quad C^* \equiv \frac{1}{B^*} = \frac{\nu_l}{BR^2}, \tag{24}$$

the weighting function can be expressed alternatively as

$$W_a = \frac{A^*\exp(-\psi/C^*)}{\sqrt{\psi}}, \tag{25}$$

which is a generalization of the form used in the authors' smooth-walled paper [11]. From this equation it may be seen that C^* has the nature of a relaxation time. It is the non-dimensional time required for the numerator of Eq. (25) to reduce by a factor of 1/e.

4.3. *Influence of Reynolds number and roughness size*

The values of A^* and C^* depend upon the Reynolds number of the frozen-viscosity distribution (denoted herein by $\mathbf{Re}_v$) and on the roughness size k_s. Their dependencies are depicted in Figs. 3 and 4, which show families of curves loosely resembling partial Moody curves for quasi-steady skin friction coefficients. The resemblance is achieved by using $A^*/\sqrt{\mathbf{Re}_v}$ and $(C^*\,\mathbf{Re}_v)^{-1}$ as ordinates rather than A^* and C^*, thereby ensuring horizontal asymptotes at sufficiently large values of $\mathbf{Re}_v$ and k_s/D. The curves are curtailed at their left-hand ends where Eq. (5) is at its limit of validity (i.e., the roughness Reynolds number k_s^+ is equal to 70).

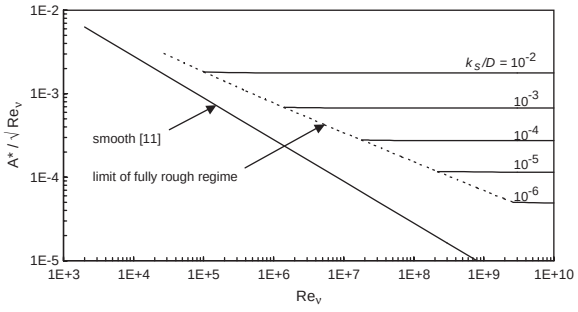

Fig. 3. Influence of the roughness ratio and the frozen Reynolds number on A^*.

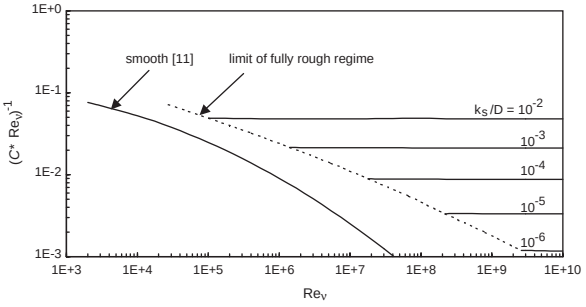

Fig. 4. Influence of the roughness ratio and the frozen Reynolds number on C^*.

For completeness, the corresponding curves are also shown for the case of smooth-walled flows [11]. In this case, A^* is a universal constant, namely $1/(2\sqrt{\pi})$ independent of the Reynolds number.

Figs. 5a and b illustrate the influence of $\mathbf{Re}_v$ and k_s/D on the weighting function. In all cases, the weighting function decreases strongly with increasing ψ, confirming that the unsteady contribution to the shear stress is more influenced by recent velocity changes than by earlier ones.

The figures show the influence of (i) $\mathbf{Re}_v$ at constant k_s/D and (ii) k_s/D at constant $\mathbf{Re}_v$. At sufficiently small historical times, the weighting function at constant k_s/D increases with increasing Reynolds number. At sufficiently large times, it decreases with increasing Reynolds number. That is, the relative importance of short times compared with long times is even more pronounced at high Reynolds numbers than at small ones.

A similar behaviour can be seen for the roughness size. At sufficiently small historical times, the weighting function at constant $\mathbf{Re}_v$ increases with increasing roughness size. At sufficiently large times, it decreases with increasing roughness size. That is, the relative importance of short times compared with long times is even more pronounced at high roughness sizes than at small ones.

The Reynolds number used in these figures (and later ones) is the value for which the frozen-viscosity distribution was chosen. Usually, it will differ from the local value of the Reynolds number at any instant in the unsteady flow. Often, it will be assumed equal to the Reynolds number of a pre-existing steady flow.

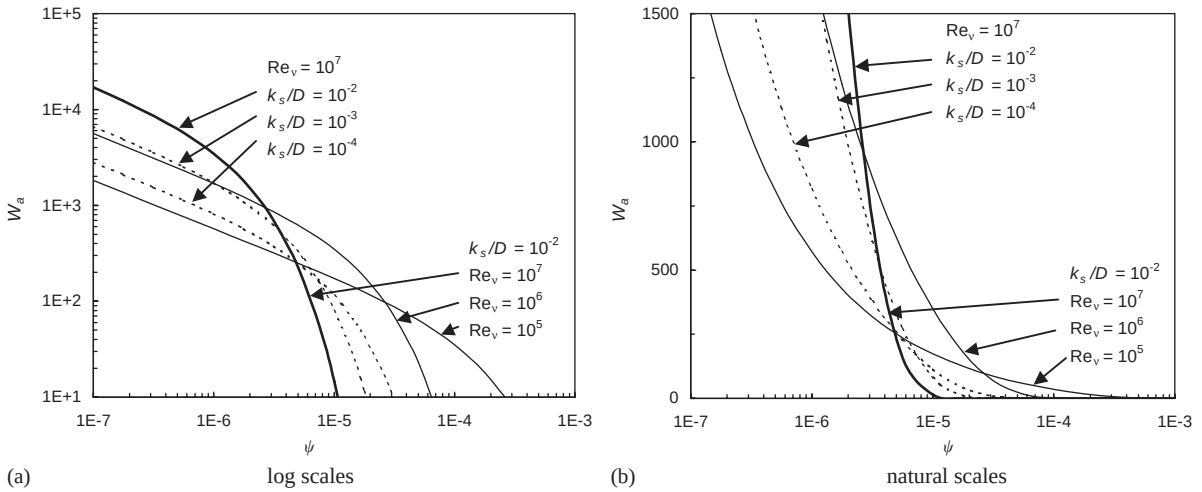

Fig. 5. Approximate weighting functions: influence of roughness ratio and frozen Reynolds number.

4.4. Interpolation formulae for A^* and C^*

At any point (x, t) in a practical simulation of an unsteady flows in a pipe network, an analyst wishing to use the weighting function given herein needs to know the values of A^* and C^*. The first step is to choose appropriate values of $\mathbf{Re}_v$ and k_s/D. Then, the corresponding values of A^* and C^* may be deduced from charts such as Figs. 3 and 4 or from tabulated versions thereof. Most analysts, however, will find it more convenient to use numerical formulae than to interpolate from tables. For this purpose, the following expressions are proposed:

$$A^* \approx 0.0103\sqrt{\mathbf{Re}_v}\left(\frac{k_s}{D}\right)^{0.39}, \tag{26}$$

$$\frac{1}{C^*} \approx 0.352\,\mathbf{Re}_v\left(\frac{k_s}{D}\right)^{0.41}. \tag{27}$$

These expressions have been deduced by a regression analysis followed by trial and error adjustment to give coefficients and exponents with few significant figures. Their maximum errors are about 4% and 10%, respectively, over the roughness size range $10^{-6} < k_s/D < 10^{-2}$. The average errors are considerably smaller.

5. Uniform acceleration

5.1. Unsteady skin friction coefficient

In the special case of a uniform acceleration $\partial U/\partial t = \dot{U}_0$, say, the use of the approximate weighting function (Eq. (25)), enables the wall shear stress to be obtained by an analytic

integration of Eq. (13). The result can be arranged in the form of an unsteady skin friction coefficient f_u as

$$f_u \equiv \frac{\tau_{wu}}{\frac{1}{2}\rho \dot{U}_0 R} \approx 4A^* \sqrt{\pi C^*}\ \mathrm{erf}\{\sqrt{\Psi/C^*}\}, \tag{28}$$

in which erf{ } is the error function and Ψ is the non-dimensional time corresponding to T, the interval since the flow was stationary.

For any particular roughness ratio and frozen Reynolds number, the coefficients A^* and C^* are constants and so Eq. (28) shows that the shape of the unsteady shear stress history is determined by the error function. When $\Psi = 0$, the unsteady skin friction coefficient f_u is zero. When Ψ is large, f_u approaches a limiting value f_{uL} given by

$$f_{uL} = 4A^* \sqrt{\pi C^*}. \tag{29}$$

Fig. 6 illustrates the development of the unsteady skin friction coefficient during uniform accelerations with the same roughness sizes and frozen Reynolds numbers as in Fig. 5. It can be seen that the limiting value f_{uL} is independent of $\mathbf{Re}_v$, but that it is strongly dependent upon k_s/D. The dependence is illustrated in more detail in Fig. 7.

5.2. Rise time Ψ_L

Fig. 6 also shows that the time required to approach the limiting value f_{uL} depends more strongly on $\mathbf{Re}_v$ than on k_s/D (see also Fig. 8). The duration of the period of increasing f_u can be quantified by noting that the error function attains values of 0.95 and 0.99 when its argument is equal to 1.386 and 1.821, respectively. Hence, Eq. (28) shows that the non-dimensional rise times to 95% and 99% of the limiting unsteady contribution to the shear stress are

$$\Psi_{0.95L} = 1.921C^* \quad \text{and} \quad \Psi_{0.99L} = 3.317C^*. \tag{30}$$

When these times are small in comparison with time scales of flow unsteadiness, numerical analysts may disregard variations in f_u and use the approximation $f_u = f_{uL}$ at all times. In contrast, when the time scales of flow unsteadiness are small in comparison with the rise time,

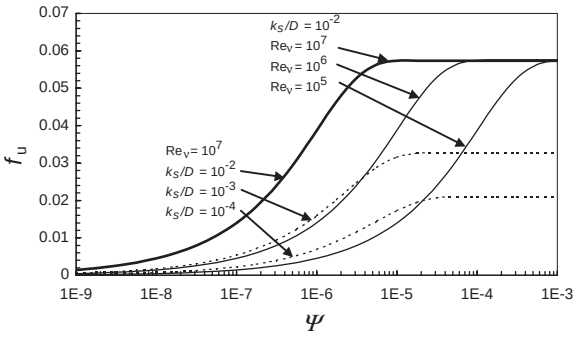

Fig. 6. Growth of the unsteady skin friction coefficient during uniform acceleration: influence of the roughness ratio and the frozen Reynolds number.

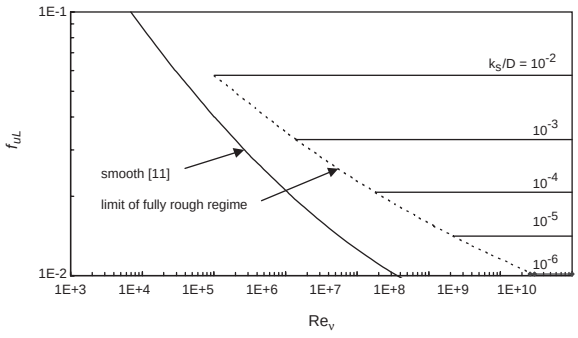

Fig. 7. Influence of the roughness ratio and the frozen Reynolds number on the limiting unsteady skin friction coefficient (and hence on Brunone's coefficient k_3).

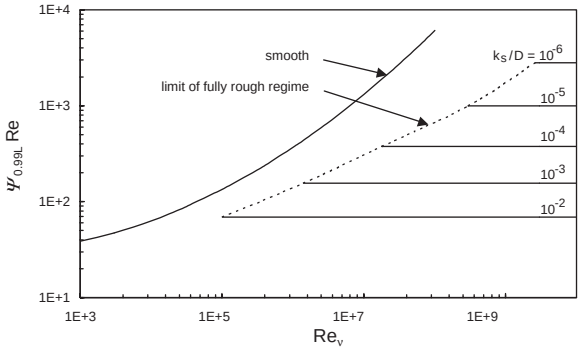

Fig. 8. Time to approach limiting unsteady shear stress conditions: influence of roughness ratio and frozen Reynolds number.

account must be taken of the time-dependent nature of f_u. This is the case, for instance, when investigating evolving shapes of a pressure wave front as it tends to develop towards a shock.

For completeness, note that the numerical values in Eq. (30) have been obtained using commercially available mathematics software. They differ slightly from values reported previously by the authors [10,11] using standard tables requiring relatively coarse interpolation.

5.3. *Brunone coefficient* k_3

For the particular case of uniform acceleration in space and time, the limiting unsteady friction coefficient f_{uL} can be shown [21] to be equal to the parameter k_3 used by Brunone et al. [19,26] in their instantaneous-acceleration representation of unsteady skin friction. Although the match is demonstrated only for the particular case of uniform acceleration, its implications extend to more general unsteady flows.

In analyses based on the instantaneous-acceleration method, it is usual to regard k_3 as a constant for any particular pipe. Some analysts have taken account of a dependence on the Reynolds number—i.e., $k_3 = k_3\{\mathbf{Re}_v\}$—but the authors are not aware of any studies in which k_3

has been regarded as dependent upon the acceleration. It follows that the value obtained for one flow state in any particular system is implicitly regarded as valid for all other flow states in the system. In particular, values obtained for f_{uL} in uniformly accelerating flows may also be interpreted as predicted values of k_3 in non-uniformly accelerating flows, provided only that the values of k_s/D and $\mathbf{Re}_v$ are unchanged.

5.4. *Influence of* $\mathbf{Re}_v$ *and* k_s/D *on* f_{uL}

Fig. 7 illustrates the dependence of f_{uL} (and hence k_3) on the frozen Reynolds number, predictions being shown for a range of roughness ratios. The curves are curtailed at their low Reynolds number ends where the roughness Reynolds number k_s^+ is equal to 70.

By inspection, f_{uL}, like its quasi-steady counterpart f_s, is independent of $\mathbf{Re}_v$ in the fully rough region. In the case of f_{uL}, the implication is that the unsteady shear stress due to any particular acceleration is independent of $\mathbf{Re}_v$. In the case of f_s, however, the implication is that the quasi-steady shear stress increases with $\mathbf{Re}_v^2$. It follows that the relative importance of unsteady skin friction in any particular pipe will usually reduce strongly with increasing Reynolds number.

Fig. 7 shows that f_{uL} increases with increasing roughness, as does its quasi-steady counterpart (see Eq. (5)). In practice, a 10-fold increase in k_s/D implies increases of about 50% in f_{uL} and of about 150% in f_s. Thus, the relative importance of unsteady skin friction at any particular Reynolds number decreases with increasing roughness.

5.5. *Influence of* $\mathbf{Re}_v$ *and* k_s/D *on* Ψ_L

Fig. 8 shows the dependence of the rise time $\Psi_{0.99L}$ on the frozen Reynolds number for a range of roughness ratios. The ordinate is chosen as $\Psi_{0.99L}\mathbf{Re}_v$ instead of $\Psi_{0.99L}$ alone because, for any particular roughness ratio, $\Psi_{0.99L}$ is found to be inversely proportional to $\mathbf{Re}_v$. As a consequence, graphs of $\Psi_{0.99L}\mathbf{Re}_v$ versus $\mathbf{Re}_v$ are horizontal lines for fully rough-walled flows.

The larger the Reynolds number, the smaller $\Psi_{0.99L}$. That is, the smaller the period during which differences between f_u and f_{uL} are significant. Indeed, since $\Psi_{0.99L}$ is inversely proportional to $\mathbf{Re}_v$, a 10-fold increase in $\mathbf{Re}_v$ implies a 10-fold decrease in the rise time. It follows that instantaneous-acceleration representations of unsteady skin friction will tend to be increasingly accurate as $\mathbf{Re}_v$ increases.

Fig. 8 shows that, for any particular value of $\mathbf{Re}_v$, the rise time $\Psi_{0.99L}$ also decreases with increasing roughness. Typically, for any particular value of $\mathbf{Re}_v$, a 10-fold increase in roughness induces an approximately 2.5-fold decrease in the rise time. Thus, the biggest rise times occur at small Reynolds numbers and small roughness ratios.

It may be deduced that rise times are more likely to be significant in small-scale laboratory studies than in large-scale engineering practice. Even in the latter case, however, they will not always be small. In the long-pipe results presented by Brunone [26], for instance, the non-dimensional rise time corresponding to $\mathbf{Re}_v = 390\,000$ and $k_s/D = 0.0088$, is approximately $\Psi_{0.99L} = 10^{-4}$, implying a physical time of 1.5 s. By comparison, the duration of the pressure fall on pump shut down is about 1 s. This explains why the shapes of the steepest parts of the measured pressure histories are not reproduced accurately by instantaneous-acceleration methods even if damping is well predicted overall.

5.6. Comparison with numerical calculations of Pezzinga

The predictions in Fig. 7 can be compared with alternative predictions due to Pezzinga [14], who developed a quasi-2D numerical model based on a laminar layer surrounding a turbulent core satisfying mixing length criteria. The flow region is discretized as a series of concentric cylindrical shells, in each of which the shear stress is expressed using either Newtonian laminar viscosity or Prandtl's mixing length expression. The mixing length is allowed to decay exponentially with distance from the wall and the von Karman 'constant' is correlated with the experimental data of Nikuradse.

Pezzinga [15] later used his quasi-2D analysis to simulate unsteady flows in a pipeline following the sudden closure of a valve at its downstream end. He undertook the analyses for a range of initial Reynolds numbers $\mathbf{Re}_0$ and roughness size ratios k_s/D. For each combination of $\mathbf{Re}_0$ and k_s/D, he also undertook a series of 1D analyses using a range of values of the parameter k_3. By comparing the results from the two types of analysis, he was able to deduce the most suitable value suitable values of k_3. This enabled him to explore the dependence of k_3 on $\mathbf{Re}_0$ and k_s/D.

Pezzinga found that, for any particular values of k_s/D and the initial Reynolds number, his results could be expressed in the form of charts that are qualitatively similar to Fig. 7 (except that they include data for flows between the extremes of fully smooth and fully rough). However, he found that different charts were obtained for alternative values of a characteristic pipe parameter denoted herein by y_{pez} and equivalent to

$$y_{pez.} \equiv 2f_s \frac{L}{D}\frac{U}{a}, \tag{31}$$

where L is the pipe length and a is the wave speed (NB: Pezzinger used the symbol y_0, not y_{pez}).

It is not easy to deduce a physical meaning for the parameter y_{pez} from Pezzinga's paper alone. Consider, however, a steady flow with a prescribed velocity U in a pipe of known diameter D and quasi-steady skin friction coefficient f_s. For this case, y_{pez} will scale with L/a, which is the time required for a wave front to traverse the pipe. As noted by Mansour et al. [16], the behaviour of unsteady skin friction stresses depends upon the relative magnitudes of L/a and the time required for vorticity diffusion in the cross-section. The latter is closely related to the limit times given by Eq. (30). With sufficiently small L/a, successive wave fronts will arrive at any particular position along a pipe within the relevant limit time and so the shear stresses will depend upon L/a (and hence upon y_{pez}). With much longer times, however, the dependence will reduce.

Pezzinga provided additional evidence in support of this interpretation. He noted that the optimum value of k_3 appeared to vary with the position along the pipe. This is to be expected because the minimum interval between successive reflections of the primary wave front varies along the pipe. It varies from L/a at the mid-length of the pipe to zero at each end. Sufficiently close to a pipe end, the interval between successive reflections from that end will always be smaller than the limit time.

Subject to the above interpretation, Pezzinga's results can be used to support the predicted dependence of the limit time on the Reynolds number. For the particular case of a nearly smooth pipe, a five-fold increase in y_{pez} had little influence on the unsteady skin friction coefficient when $\mathbf{Re}_v = 10^8$, but the same increase had a large influence when $\mathbf{Re}_v = 10^4$. This suggests that the rise

time at $\mathbf{Re}_v = 10^8$ is smaller than that at $\mathbf{Re}_v = 10^4$, which is consistent with the trend predicted above.

6. The need for experimental evidence

At present, there is no definitive experimental information on transient wall shear stresses in rough-walled pipes. There is a need for detailed experimental data to confirm (or deny) the validity of the predicted theoretical values of the weighting functions and the consequential values of the instantaneous-acceleration parameter k_3.

The present position for rough-walled flows is broadly similar to the position that pertained for smooth-walled flows when the authors presented their predictions for smooth-walled flows [10]. Subsequent experimental work by other researchers, e.g., Bergant et al. [22,23], Bughazem and Anderson [24] and Vitkovsky et al. [25] has shown reasonable agreement with those predictions. The authors hope that future experiments will give similar support to the rough-walled predictions presented herein. In the meantime, however, they can only wait.

7. Conclusions

1. The wall shear stress in a pipe under fully rough conditions has been determined for general unsteady flows, based on an assumed viscosity distribution in the pipe cross-section. The distribution has many features in common with a previous model for smooth-walled pipes [11], namely:
   (a) in an outer annular region, the viscosity varies linearly from a minimum at the wall to a maximum at the interface with the core region;
   (b) in a central core, the viscosity is assumed uniform and equal to that in a steady flow for a predefined Reynolds number $\mathbf{Re}_v$ and roughness size k_s; and
   (c) in both regions, the viscosity is assumed constant in time for the duration of the transient.
2. The viscosity in the core region is assumed equal to $0.065u_* R$. The viscosity at the wall is obtained by matching the implied skin friction with widely used formulae for steady, rough-walled flows. It is always greater than the laminar viscosity.
3. With these assumptions, the unsteady shear stress is found to depend on a weighted integral over the acceleration history. A simple analytical expression has been found that closely approximates the predicted weighting function.
4. The approximate weighting function—and hence the wall shear stress—has been shown to depend on two parameters A^* and C^* which are unique for any particular combination of the frozen Reynolds number $\mathbf{Re}_v$ and the pipe roughness ratio k_s/D. Approximate interpolation functions have been presented, enabling values of A^* and C^* to be estimated in numerical simulations of transient flows.
5. During uniform acceleration, the unsteady skin friction coefficient increases towards a limiting value f_{uL} which increases with increasing roughness, but is independent of the Reynolds number. The time required to approach the limiting value decreases with increasing roughness and with increasing Reynolds number.

6. Consideration of the special case of a flow accelerating uniformly in space and time enables the limiting unsteady skin friction coefficient f_{uL} to be interpreted as identical to the coefficient k_3 used in a popular instantaneous-acceleration model of unsteady skin fiction presented by Brunone et al. [19,26].

Appendix A. Unsteady flow analysis

The analytical development closely follows the corresponding analysis for smooth-walled flows [11]. It is presented in summary form, enabling the influence of roughness to be illustrated without excessive detail.

A.1. Governing equations

The assumed viscosity distribution may be expressed as

$$\begin{aligned} &\textit{Annulus}: \quad v = v_w(1+\alpha y), \\ &\textit{Core}: \quad v = v_c, \end{aligned} \tag{A.1}$$

where α, the fractional rate of change of viscosity with distance y from the wall, satisfies

$$\alpha = \frac{v_c - v_w}{b v_w} = \frac{(\sigma_{cw} - 1)}{b}. \tag{A.2}$$

The equations of motion in the annulus and the core are, respectively,

$$\frac{\partial u}{\partial t} = -P + \frac{\partial}{\partial y}\left(v(y)\frac{\partial u}{\partial y}\right) \tag{A.3}$$

and

$$\frac{\partial u}{\partial t} = -P + \frac{v_c}{r}\frac{\partial}{\partial r}\left(r\frac{\partial u}{\partial r}\right), \tag{A.4}$$

in which

$$P \equiv \frac{1}{\rho}\frac{\partial p}{\partial x} - \frac{\mathrm{d}Z}{\mathrm{d}x}. \tag{A.5}$$

In the above equations, $u\{x, y, t\}$ is the velocity in the axial direction x in the annulus, $u\{x, r, t\}$ is the velocity in the axial direction x in the core, p is the pressure and Z is a gravitational potential.

The boundary conditions are

$$\begin{aligned} &\textit{Annulus}: \quad u_{y=0} = 0, \quad u_{y=b} = u_{MA}, \\ &\textit{Core}: \quad (\partial u/\partial r)_{r=0} = 0, \quad u_{r=R-b} = u_{MC}, \end{aligned} \tag{A.6}$$

in which b is the width of the annulus and the suffix M denotes the interface between the annulus (A) and the core (C).

The matching conditions at the annulus/core interface are

$$\begin{aligned} &\textit{Velocity}: \quad u_{MA} = u_{MC} \equiv u_M, \\ &\textit{Shear stress}: \quad (\partial u/\partial y)_{y=b} = -(\partial u/\partial r)_{r=R-b}. \end{aligned} \tag{A.7}$$

The assumed initial condition is that the velocity is zero everywhere:

$$\begin{aligned} &\textit{Annulus}: \quad u\{x, y, 0\} = 0, \\ &\textit{Core}: \quad u\{x, r, 0\} = 0. \end{aligned} \tag{A.8}$$

A.2. Transformed velocity distribution

After Laplace transformation, Eqs. (A.3) and (A.4) are solved subject to the transforms of conditions (A.6)–(A.8) to obtain the transformed velocity distributions in the annulus and the core, namely,

$$u'(\eta) = [C_1 \mathrm{I}_0(\eta) + C_2 \mathrm{K}_0(\eta) - 1](P'/s) \tag{A.9}$$

and

$$u'(r) = \left[\frac{(1+H)\mathrm{I}_0(r\sqrt{s/v_c})}{\mathrm{I}_0(r_M\sqrt{s/v_c})} - 1\right]\frac{P'}{s}, \tag{A.10}$$

respectively, where I_0 and K_0 are modified Bessel functions of the first and second kinds and zero order, s is the Laplace transform parameter and

$$\eta \equiv \frac{2}{\alpha}\sqrt{\frac{s}{v_w}[1+\alpha y]}. \tag{A.11}$$

The parameters C_1, C_2 and H in these equations are constants for any particular pipe and any particular value of the Laplace parameter s. The matching conditions at the annulus/core interface (Eq. (A.7)) enable the following relationships to be found between them:

$$C_1 = A_3 + A_5 H = -\frac{1}{\Delta}[\mathrm{K}_0(\sqrt{\zeta})(1+H) - \mathrm{K}_0(\sqrt{\sigma_{cw}\zeta})], \tag{A.12}$$

$$C_2 = A_4 + A_6 H = -\frac{1}{\Delta}[\mathrm{I}_0(\sqrt{\sigma_{cw}\zeta}) - \mathrm{I}_0(\sqrt{\zeta})(1+H)] \tag{A.13}$$

and

$$H \equiv \frac{M(r_M\sqrt{s/v_c}) + A_3\mathrm{I}_1(\sqrt{\sigma_{cw}\zeta}) - A_4\mathrm{K}_1(\sqrt{\sigma_{cw}\zeta})}{M(r_M\sqrt{s/v_c}) + A_5\mathrm{I}_1(\sqrt{\sigma_{cw}\zeta}) - A_6\mathrm{K}_1(\sqrt{\sigma_{cw}\zeta})}, \tag{A.14}$$

in which

$$\zeta \equiv ([\eta]_{y=0})^2 = \frac{4s}{\alpha^2 v_w}, \tag{A.15}$$

$$\Delta \equiv \mathrm{I}_0(\sqrt{\zeta})\mathrm{K}_0(\sqrt{\sigma_{cw}\zeta}) - \mathrm{K}_0(\sqrt{\zeta})\mathrm{I}_0(\sqrt{\sigma_{cw}\zeta}) \tag{A.16}$$

and

$$M(z) \equiv \frac{\mathrm{I}_1(z)}{\mathrm{I}_0(z)}. \tag{A.17}$$

A.3. Transformed shear stress

The transformed shear stress τ' can be obtained by differentiating Eqs. (A.9) and (A.10) and multiplying by the appropriate dynamic viscosity. This gives the dependence of τ' on the transformed pressure gradient P'. For most transient analyses, however, it is more convenient to relate the shear stress to the mean velocity history. Therefore, it is useful to eliminate P' from Eqs. (A.9) and (A.10) in favour of the transformed mean velocity U'.

The transformed volumetric rates of flow in the annulus (Q'_A) and core (Q'_C) regions are obtained by integrating Eqs. (A.9) and (A.10), giving

$$\frac{Q'_A}{2\pi(r_M + 0.5b)} \approx \int_0^b u'(y)\,\mathrm{d}y = \frac{\alpha v_w}{2s}\left[C_1\eta\mathrm{I}_1(\eta) - C_2\eta\mathrm{K}_1(\eta) - \frac{\eta^2}{2}\right]_{\sqrt{\zeta}}^{\sqrt{\sigma_{cw}\zeta}} \frac{P'}{s} \tag{A.18}$$

and

$$Q'_C = 2\pi \int_0^{r_M} u'(r) r\,\mathrm{d}r = [2\pi r_M \sqrt{v_c/s}(1+H)[\mathrm{I}_1(r_M\sqrt{s/v_c})]/[\mathrm{I}_0(r_M\sqrt{s/v_c})] - \pi r_M^2]\frac{P'}{s}, \tag{A.19}$$

respectively, in which r_M, the radius at the interface, is equal to $R - b$. These equations show that P' is linearly proportional to the transformed mean velocity, satisfying

$$\frac{P'}{s} = GU' = G\frac{(Q'_A + Q'_C)}{\pi R^2}, \tag{A.20}$$

in which G can be determined by comparing Eq. (A.20) with Eqs. (A.18) and (A.19).

The shear stress at any location in the annular region satisfies $\tau = \rho\nu(\partial u/\partial y)$. Using Eqs. (A.9) and (A.20), the transformed shear stress at the wall is found to be related to the transformed mean velocity by

$$\tau'_w = \rho v_w(\sqrt{s/v_w})[C_1\mathrm{I}_1(\sqrt{\zeta}) - C_2\mathrm{K}_1(\sqrt{\zeta})]GU', \tag{A.21}$$

where I_1 and K_1 are modified Bessel functions of the first and second kinds and first order.

Appendix B. Steady flow analysis

The unsteady flow analysis presented in Appendix A yields the transformed shear stress at any instant during an unsteady flow. It is useful to regard this as the sum of a steady state component and an additional component attributable to unsteadiness. This appendix includes the derivation of the relevant steady state component. The analysis is undertaken in the physical domain and the final result is transformed into the Laplace domain.

The equations of steady state flow can be obtained from Eqs. (A.3) and (A.4) by setting the time derivative of velocity to zero and interpreting all other quantities as independent of time. By following a similar procedure to that used in Appendix A for unsteady flows, the velocity

distributions in the annulus and the core can be shown to be

$$u(y) = \frac{Pb^2}{(\sigma_{cw}-1)v_w}\left(\frac{y}{b} - \frac{\ln(1+\alpha y)}{\ln \sigma_{cw}}\right) + u_M \frac{\ln(1+\alpha y)}{\ln \sigma_{cw}} \tag{B.1}$$

and

$$u(r) = -\frac{P(r_M^2 - r^2)}{4v_c} + u_M, \tag{B.2}$$

respectively, where u_M, the velocity at the interface between the annulus and the core, is

$$u_M = -\frac{Pb^2 \ln \sigma_{cw}}{v_w(\sigma_{cw}-1)}\left[\frac{r_M}{2b} + \frac{\sigma_{cw}}{(\sigma_{cw}-1)} - \ln \sigma_{cw}\right]. \tag{B.3}$$

The volumetric rates of flow in the annulus and core regions are obtained by integrating Eqs. (B.1) and (B.2), giving

$$Q_{A,s} = -\frac{(2\pi r_M + b/2)}{\alpha^2 v_w}\left(\left[\frac{r_M}{2} + \frac{\sigma_{cw}}{\alpha}\right](\sigma_{cw}\ln\sigma_{cw} - \sigma_{cw} + 1) - (\alpha b^2/2)\right)P \tag{B.4}$$

and

$$Q_{C,s} = -\frac{\pi r_M^2}{\alpha^2 v_w}\left(\frac{\alpha^2 r_M^2}{8\sigma_{cw}} + (\ln \sigma_{cw})[(\alpha r_M/2) + \sigma_{cw}] - \sigma_{cw} + 1\right)P, \tag{B.5}$$

respectively, in which the suffix s denotes steady flow.

The pressure gradient can now be related to the mean velocity U_s by

$$P = G_s U_s = G_s \frac{(Q_{A,s} + Q_{C,s})}{\pi R^2}, \tag{B.6}$$

in which the parameter G_s can be inferred by comparing Eq. (B.6) with Eqs. (B.4) and (B.5).

The shear stress at any location is obtained by differentiating Eq. (B.1) or (B.2). Using Eq. (B.6), the dependence of the shear stress at the wall on the mean velocity is found to satisfy

$$\tau_{ws} = -\rho\left[\frac{r_M}{2} + b\right] G_s U_s. \tag{B.7}$$

The Laplace transform of this steady state wall shear stress is

$$\tau'_{ws} = -\rho\left[\frac{r_M}{2} + b\right] G_s U_s. \tag{B.8}$$

Appendix C. Nomenclature

a	wave speed
A	parameter defining the approximate weighting function (Eq. (19))
$A_3, A_4, , A_5, , A_6$	quantities defined implicitly in Eqs. (A.12) and (A.13)
b	width of annular region
B	parameter defining the approximate weighting function (Eq. (19))
C^*	shear decay coefficient defined in Eq. (24)
C_1	composite quantity defined in Eq. (A.12)
C_2	composite quantity defined in Eq. (A.13)

D	diameter of pipe
f	skin friction coefficient
G	parameter relating the driving force and the mean velocity (see Eq. (A.20))
H	parameter relating the driving force and the matching velocity (see Eq. (A.14))
I_n	modified Bessel function of first kind and nth order
k_s	roughness size
k_3	coefficient in Brunone's instantaneous-acceleration model
K_n	modified Bessel function of second kind and nth order
L	length of pipe
N_c	core viscosity matching constant
M	function defined by Eq. (A.17)
p	pressure
P	'driving force' defined by Eq. (A.5)
Q	volume flow rate
r, Θ, x	polar co-ordinates—radial, angular and axial
r_M	radius at annulus/core interface ($= R - b$)
R	pipe radius
Re	Reynolds number
$\mathbf{Re}_v$	frozen Reynolds number defining the viscosity distribution
s	Laplace transform parameter
t	time
T	time since the disturbance began
u	fluid velocity in the axial (x) direction
u_*	friction velocity
U	mean velocity in the cross-section
$\dot{U}_0$	prescribed acceleration in the cross-section
W	weighting function
x, y	Cartesian co-ordinates—axial axial lateral
$y_{pez.}$	parameter y_0 used by Pezzinga [15]
z	argument of function
Z	body force potential
α	lateral rate of change of viscosity in annulus
β	ratio of annulus thickness to pipe radius
Δ	function defined by Eq. (A.16)
ζ	value of η^2 at the wall (see Eq. (A.15))
η	similarity variable (Eq. (A.11))
θ	historical time
ν	kinematic or eddy viscosity (distinguished by subscript)
ρ	fluid density
σ_{ab}	ratio ν_a/ν_b where a, b denote core, laminar, wall, etc.
τ_w	shear stress at the pipe wall
Φ_u	function relating mean velocity and unsteady wall shear stress transforms
ψ	non-dimensional time defined by Eq. (24)
Ψ	non-dimensional time since disturbance began

Subscripts

a	approximate quantity
A	annulus
c, C	core region
l	laminar
L	limiting condition
M	matching condition at annulus/core interface
s	quasi-steady
T	time
u	unsteady
w	wall
0	asymptotic point

Superscripts

$+$	non-dimensional with respect to friction velocity and laminar kinematic viscosity
$'$	Laplace transformed quantity

References

[1] W. Zielke, Frequency dependent friction in transient pipe flow, *Journal of Basic Engineering, Transactions of the American Society of Mechanical Engineers Series D* 90 (1968) 109–115.

[2] H. Arlt, Experimentelle Untersuchung über die instationäre turbulente Reibungsverhalten bei aufegprägten Druckimpulsen in einer Rohrleitung mit Kreisquerschnitt, Mitteilung No. 102, Institut für Wasserbau und Waserwissenchaft, Technische Universität Berlin, 1983.

[3] E.L. Holmboe, W.T. Rouleau, The effect of viscous shear on transients in liquid lines, *Journal of Basic Engineering, Transactions of the American Society of Mechanical Engineers* 89 (1967) 174–180.

[4] S. Ozawa, T. Maeda, T. Matsumura, K. Nakatani, K.Uchida, Distortion of compression wave during propagation along Shinkansen tunnel, *Eighth International Conference on the Aerodynamics and Ventilation of Vehicle Tunnels*, BHR Group, Liverpool, UK, 6–8 July 1994, pp. 211–226.

[5] M. Ohmi, T. Usui, Pressure and velocity distributions in pulsating turbulent pipe flow Part 1: theoretical treatment, *Bulletin JSME* 19 (1976) 307–313.

[6] M. Ohmi, S. Kyomen, T. Usui, Numerical analysis of transient turbulent flow in liquid lines, *Bulletin JSME* 28 (1985) 799–806.

[7] P. Eichinger, G. Lein, The influence of friction on unsteady pipe flow, *International Conference on Unsteady Flow and Fluid Transients*, HR Wallingford, Durham UK, 1992, pp. 41–50.

[8] A.E. Vardy, K.L. Hwang, J.M.B. Brown, A weighting function model of transient turbulent pipe friction, *Journal of Hydraulic Research* 31 (1993) 533–544.

[9] D.J. Wood, J.E. Funk, A boundary-layer theory for transient viscous losses in turbulent flow, *Journal of Basic Engineering, Transactions of the American Society of Mechanical Engineers* 92 (1970) 865–873.

[10] A.E. Vardy, J.M.B. Brown, Transient, turbulent, smooth pipe friction, *Journal of Hydraulic Research* 33 (1995) 435–456.

[11] A.E. Vardy, J.M.B. Brown, Transient turbulent friction in smooth pipe flows, *Journal of Sound and Vibration* 259 (2003) 1011–1036.

[12] Z. Zarzycki, On weighting function for wall shear stress during unsteady turbulent pipe flow, *Eighth International Conference on Pressure Surges*, BHR Group, The Hague, Netherlands, 2000, pp. 529–543.

[13] W.F. Silva-araya, M.H. Chaudry, Unsteady friction in rough pipes, *Journal of Hydraulic Engineering, American Society of Civil Engineers* 127 (7) (2001) 607–618.

[14] G. Pezzinga, Quasi-2D model for unsteady flow in pipes, *Journal of Hydraulic Engineering, American Society of Civil Engineers* 125 (7) (1999) 676–685.
[15] G. Pezzinga, Evaluation of unsteady flow resistance by quasi-2D or 1D models, *Journal of Hydraulic Engineering, American Society of Civil Engineers* 126 (10) (2000) 778–785.
[16] M.S. Ghidaoui, S.G.S. Mansour, M. Zhao, Applicability of quasisteady and axisymmetric turbulence models in water hammer, *Journal of Hydraulic Engineering, American Society of Civil Engineers* 128 (10) (2002) 917–924.
[17] A.K. Trikha, An efficient method for simulating frequency-dependent fiction in transient liquid flow, *Journal of Fluids Engineering, Transactions of the American Society of Mechanical Engineers* 97 (1975) 97–105.
[18] M.S. Ghidaoui, S. Mansour, Efficient treatment of the Vardy–Brown unsteady shear in pipe transients, *Journal of Hydraulic Engineering, American Society of Civil Engineers* 128 (1) (2002) 102–112.
[19] B. Brunone, U. Golia, M. Greco, Modelling of fast transients by numerical methods, *Proceedings of the Ninth Round Table Meeting on Hydraulic Transients with Column Separation*, IAHR Group, Valencia, 1991, pp. 273–280.
[20] D.H. Axworthy, M. Ghidaoui, D.A. McInnes, Extended thermodynamics derivation of energy dissipation in unsteady pipe flow, *Journal of Hydraulic Engineering, American Society of Civil Engineers* 126 (4) (2000) 276–287.
[21] A.E. Vardy, J.M.B. Brown, On turbulent, unsteady, smooth pipe friction, *Seventh International Conference on Pressure Surges*, BHR Group, Harrogate, UK, 1996, pp. 289–311.
[22] A. Bergant, A.R. Simpson, J. Vitkovsky, Review of unsteady friction models in transient pipe flow, *The Behaviour of Hydraulic Machinery Under Steady Oscillatory Conditions*, IAHR Work Group, Ninth International Meeting, 7–9 September 1999, Brno, Czech Republic.
[23] A. Bergant, A.R. Simpson, J. Vitkovsky, Developments in unsteady pipe flow fiction modelling, *Journal of Hydraulic Research* 39 (2001) 249–257.
[24] M.B. Bughazem, A. Anderson, Investigation of an unsteady friction model for waterhammer and column separation, *Eighth International Conference on Pressure Surges*, BHR Group, The Hague, Netherlands, 2000, pp. 483–498.
[25] J. Vitkovsky, M. Lambert, A. Simpson, A. Bergant, Advances in unsteady friction modelling in transient pipe flow, *Eighth International Conference on Pressure Surges*, BHR Group, The Hague, Netherlands, 2000, pp. 471–482.
[26] B. Brunone, M. Ferrante, F. Calabresi, High Reynolds number transients in a pump rising main. Field tests and numerical modeling, *Fourth International Conference on Water Pipeline Systems*, March 2001, BHR Group, York UK, 2001 pp. 339–348.
[27] H. Schlichting, *Boundary Layer Theory*, 7th Edition, McGraw-Hill, New York, 1979.
[28] J. Laufer, The structure of turbulence in fully developed pipe flow, NACA TR 1174, 1954.
[29] S.W. Churchill, C.C. Chan, Theoretically based correlating equations for the local characteristics of fully turbulent flow in round tubes and between parallel plates, *Industrial & Engineering Chemistry Research* 34 (1995) 1332–1341.
[30] T. Maruyama, T. Kuribayashi, T. Mizushima, The structure of the turbulence in transient pipe flows, *Journal of Chemical Engineering Japan* 9 (1976) 431–439.
[31] S. He, J.D. Jackson, A study of turbulence under conditions of transient flow in a pipe, *Journal of Fluid Mechanics* 408 (2000) 1–38.
[32] S. He, J.D. Jackson, Wall shear stress in accelerating pipe flows, *International Conference on Energy Conversion and Application*, 17–20 June 2001, Wuhan, China.